Journal of
Telecommunication, Switching Systems and Networks

ISSN: 2454-6372
Volume 13, Issue 1, 2026
January–April
DOI (Journal): 10.37591/JoTSSN

https://journals.stmjournals.com/jotssn

Review JoTSSN

Performance Analysis of Cross-Slotted Patch Antenna for Wireless System Applications

L. Sarika[1,*], K. Lavanyai[2], A. Mounika[2], K. Yasashwini[2], J. Harshitha[2]

Abstract

A C-band cross-slotted microstrip patch antenna for ice and frost detection in wireless sensing applications. The antenna configurations with distinct cross-slot geometries are designed to investigate their influence on impedance matching, radiation characteristics, and sensitivity. The antennas are modeled and analyzed using Ansys High Frequency Structure Simulator (HFSS), and their dimensions are optimized using standard microstrip antenna design equations. Ice and frost accumulation on the antenna surface is identified through measurable shifts in resonant frequency, arising from variations in the surrounding effective dielectric constant. Key antenna parameters, including reflection coefficient (S_{11}), voltage standing wave ratio (VSWR), gain, bandwidth, and far-field radiation patterns, are systematically evaluated and compared. Simulation results demonstrate good matching impedance, stable radiation performance, and clear frequency shifts under different environmental conditions. The formation of ice and frost on the antenna surface modifies the surrounding medium's effective dielectric constant, causing quantifiable changes in the resonant frequency and important performance metrics. The main sensing mechanism for detecting environmental conditions is these frequency variations. Critical antenna metrics, including reflection coefficient (S_{11}), VSWR, gain, operational bandwidth, and far-field radiation patterns, are thoroughly evaluated and compared under different environmental scenarios. Strong impedance matching, steady radiation performance, and clear frequency changes corresponding to different ice and frost thicknesses are all shown by simulation findings. These results validate the suitability of the suggested cross-slotted microstrip antennas for passive detection systems functioning in cold-region applications, C-band wireless environmental monitoring, and structural health sensing. These characteristics confirm that the proposed antennas are well suited for C-band wireless environmental monitoring and passive sensing systems.

Keywords: cross-slot, ice and water detection, frequency shift sensing, wireless environmental monitoring

***Author for Correspondence**
L. Sarika
E-mail: sarikamaha@gvpcew.ac.in

[1]Assistant Professor, Department of electronics communication and engineering, GVP College of Engineering for Women, Vishakhapatnam, Andhra Pradesh, India
[2]Student, Department of electronics communication and engineering, GVP College of Engineering for Women, Vishakhapatnam, Andhra Pradesh, India

Received Date: February 25, 2026
Accepted Date: February 27, 2026
Published Date: March 18, 2026

Citation: L. Sarika, K. Lavanyai, A. Mounika, K. Yasashwini, J. Harshitha. Performance Analysis of Cross-Slotted Patch Antenna for Wireless System Applications. Journal of Telecommunication, Switching Systems and Networks. 2026; 13(1): 35–50p.

INTRODUCTION

In recent years, antennas have evolved beyond their conventional role as radiating elements to incorporate sensing functionality, resulting in antenna-based sensing platforms. These systems have gained considerable attention for applications including environmental monitoring, early warning systems, and surface condition detection. In antenna-based sensing architectures, a single antenna simultaneously performs wireless communication and sensing, where variations in environmental conditions are captured through changes in the electromagnetic response of the antenna, enabling efficient and compact system implementation [1-6].

Ice and water accumulation on an antenna surface alters the effective dielectric properties of the surrounding medium, resulting in measurable variations in parameters such as the reflection coefficient and the resonant frequency. This sensing mechanism enables the realization of compact, low-complexity systems without the need for dedicated sensing components. However, most existing antenna-based ice and frost sensors operate at lower frequency bands, leading to larger antenna sizes and increased spectral congestion, while the influence of antenna geometry on the sensing performance has not been fully addressed. The C-band at approximately 6 GHz offers several advantages for antenna-based sensing, including reduced antenna size, improved sensitivity to dielectric loading, and lower interference compared to commonly used lower frequency bands [7-9].

Among various antenna configurations, microstrip patch antennas with slot loading are particularly attractive because of their planar structure, ease of fabrication, and ability to tailor the impedance and radiation characteristics through geometric modifications. Nevertheless, the sensing behavior of cross-slotted microstrip patch antennas at 6 GHz has not been sufficiently investigated. In this study, compact cross-slotted rectangular microstrip patch antennas with different patches operating at 6 GHz were designed and analyzed for ice and water sensing applications. The antennas employ different cross-slot geometries to slightly modify the current distribution, thereby influencing both the sensing sensitivity and radiation performance. Antennas are widely used in wireless communication systems. Traditionally, antennas have been designed solely for the transmission and reception of signals. However, recent developments have introduced sensing antennas that combine sensing and communication into a single device. Ice and water accumulation on aircraft wings, wind turbines, and power lines can cause serious operational problems. Therefore, early detection is necessary. In this study, a cross-shaped slotted patch antenna was designed to detect environmental changes based on dielectric variation [10].

When water, ice, or frost accumulates on the antenna surface, the effective permittivity changes, resulting in a shift in the resonant frequency. By monitoring this frequency shift, the material state can be identified. The proposed designs were modeled using Ansys HFSS, and key parameters such as return loss, VSWR, gain, and radiation patterns were evaluated under different dielectric loading conditions. The results confirm that the proposed antenna structures are suitable for C-band wireless environmental monitoring and antenna-based sensing applications.

DESIGN METHODOLOGY

A rectangular cross-slotted microstrip patch antenna with a microstrip line feed was selected because of its simple structure, ease of fabrication, and straightforward impedance matching. The cross-slot modifies the surface current distribution, thereby enhancing the antenna performance and sensitivity. The antenna was designed to operate in the 6 GHz C-band for ice and water sensing in wireless environmental monitoring applications [11].

DESIGN PROCEDURE

Slot-Coupled Microstrip Antenna Design with Circular Patch

Figure 1 illustrates the structure of the proposed cross-slotted circular microstrip patch antenna operating at 6 GHz in the C-band. The antenna is realized using two dielectric substrates, each characterized by a relative permittivity, ε_r = 4.4, and thickness *h*. The circular radiating patch is printed on the top surface of the upper dielectric substrate, while the microstrip feeding line is placed on the bottom surface of the lower dielectric substrate. A finite ground plane is positioned between the two substrates [12, 13].

The radius of the circular patch was initially calculated to support the dominant TM_{11} mode. The effective radius of the circular patch is expressed as:

$$a_{\text{eff}} = a\sqrt{1 + \frac{2h}{\pi a s_r}\left[\ln\left(\frac{\pi a}{2h}\right) + 1.7726\right]} = 5.8$$

The resonant frequency of the circular patch is approximated by

$$f_r = \frac{1.8412\, c}{2\pi a_{\text{eff}}\sqrt{s_r}} = 6\ \text{GHz}$$

where $c$is the speed of light in free space.

Using fr = 6GHz, the initial patch radius is obtained and later optimized through full-wave electromagnetic simulation.

A cross-shaped slot is etched at the center of the circular patch to alter the surface current distribution and enable fine-tuning of the resonant frequency and impedance matching. The antenna is excited using a 50-Ω microstrip line feed, with the feed position optimized to achieve a reflection coefficient below −10 dB at the operating frequency, as shown in Figure 1. The final antenna dimensions were optimized using Ansys HFSS a rectangular microstrip patch antenna integrated with a cross-shaped slot was developed to function as a sensing element. The design procedure consists of two main stages.

1. Development of the conventional rectangular patch antenna and
2. Incorporation of a cross-slot to enhance field concentration and sensing capability.

Rectangular Patch Antenna Design

A conventional rectangular microstrip patch antenna was designed using standard transmission line model equations. The antenna is fabricated on an FR-4 substrate with relative permittivity, εr = 4.3, loss tangent tan δ = 0.025, and thickness, d = 1.53 mm. A 50 Ω microstrip feed line is used to excite the patch.

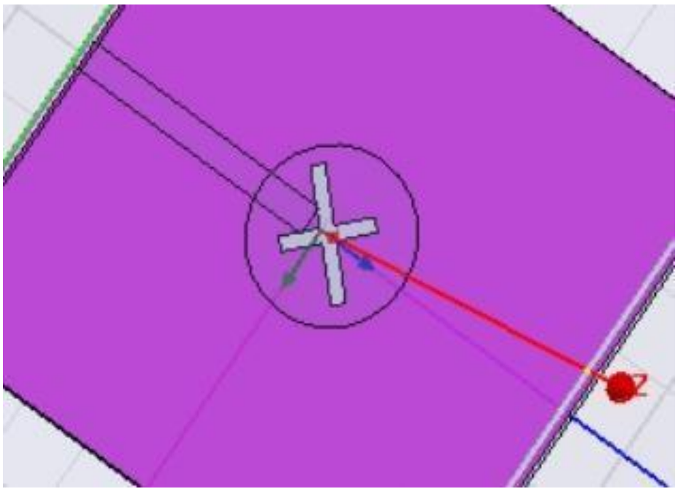

Figure 1. Slot-coupled microstrip antenna design with circular patch.

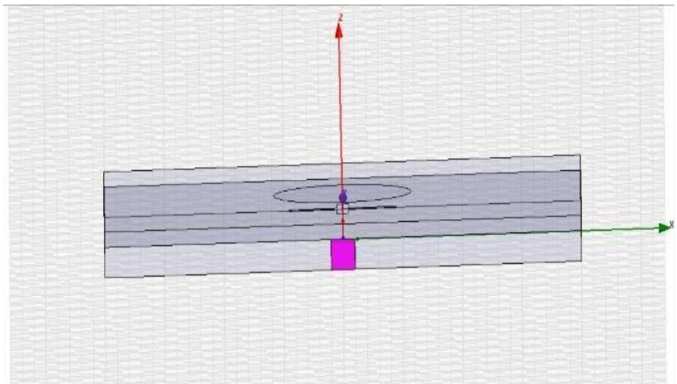

Figure 2. Cross-slot microstrip patch antenna design with rectangular patch.

The patch width $W$is calculated as:

$$W = \frac{c}{2f_r}\sqrt{\frac{2}{\varepsilon_r+1}}$$

The effective dielectric constant, $\varepsilon reff$, accounting for fringing fields, is determined by:

$$\varepsilon_{\text{reff}} = \frac{\varepsilon_r+1}{2} + \frac{\varepsilon_r-1}{2}\left(1+\frac{12d}{W}\right)^{-1/2}$$

Owing to fringing effects at the radiating edges, the antenna behaves electrically longer than its physical length. The extension in length $\Delta L$is given by:

$$\Delta L = 0.412d\ \frac{(\varepsilon_{\text{reff}}+0.3)\left(\frac{W}{d}+0.264\right)}{(\varepsilon_{\text{reff}}-0.258)\left(\frac{W}{d}+0.8\right)}$$

The effective length becomes:

$$L_{\text{eff}} = L + 2\Delta L$$

Thus, the resonant frequency is expressed as:

$$f_r = \frac{1}{2L_{\text{eff}}\sqrt{\varepsilon_{\text{reff}}\varepsilon_0\mu_0}}$$

The physical length of the patch is then calculated as:

$$L = L_{eff} - 2\Delta L$$

Using these equations, the antenna exhibits resonances near 4.8 and 5.8 GHz.

Cross-Slot Integration for Sensitivity Enhancement

To improve the sensing performance, a cross-shaped slot was etched at the center of the patch. The purpose of introducing the slot is to intensify the localized electromagnetic field distribution and increase the interaction region between the antenna surface and the Figure 2.

The cross-slot consists of two orthogonal rectangular slots. This configuration forces the surface current to follow an extended path around the slot, thereby effectively increasing the electrical length of the patch. Because the resonant frequency is inversely proportional to the effective length, this modification shifts the operating frequency downward.

The slot structure can be modeled using an equivalent, parallel capacitance network. The total equivalent capacitance is expressed as:

$$C_{eq} = C_1 + C_2$$

For identical slot arms:

$$C_1 = C_2 = C$$

Where,

- L_S and W_S are the slot length and width,
- d is the substrate thickness,
- ε is the effective permittivity,
- xf represents the feed location.

Increasing the slot dimensions increases the capacitance, which consequently lowers the resonant frequency of the device. Therefore, the slot parameters must be carefully optimized to maintain operation within the targeted frequency band.

The resonant frequency of the slot-loaded structure can be approximated using the Linear Combination (LC) model as follows:

$$f_r = \frac{1}{2\pi\sqrt{L_{eq}C_{eq}}}$$

Where, L_{eq} through full-wave electromagnetic simulations; the optimized cross-slot configuration achieves resonance near 5.8 GHz, aligning with the desired sensing band from Figure 3.

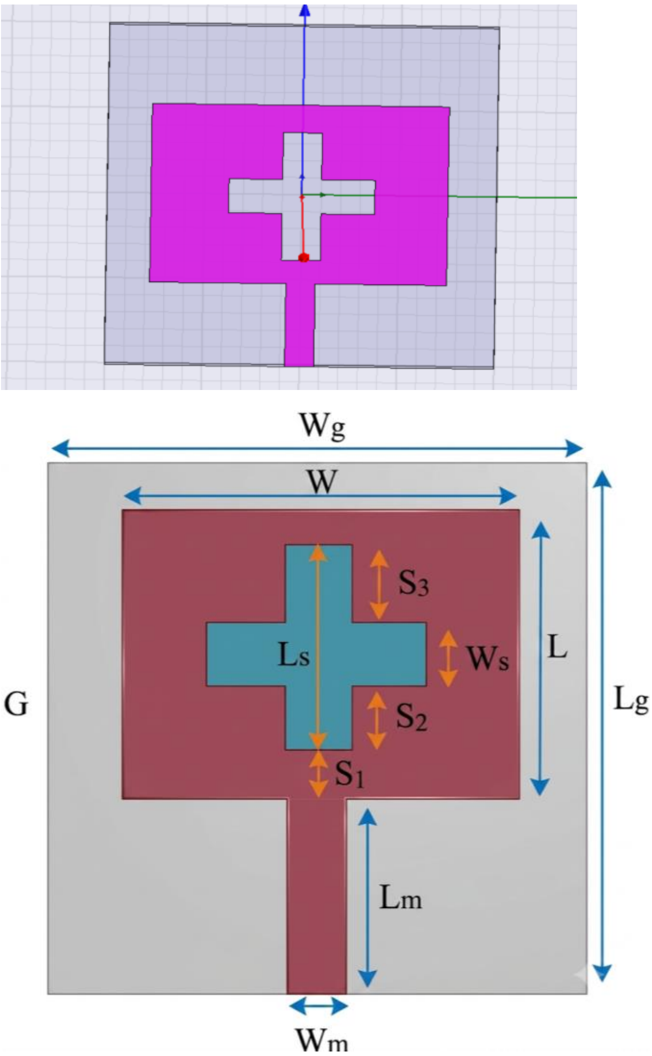

Figure 3. The proposed antenna design with a cross-shaped slot; LG = 40, WG = 40, L = 18, W = 27.5, Lm = 9.8, Wm = 3, LS = 15, WS = 4, S1 = 3, S2 = 4, S3 = 7.

SIMULATION

The proposed antenna operates as a dielectric sensor to detect water and ice accumulation. The sensing mechanism is based on monitoring the variations in the resonant frequency. When a dielectric layer is introduced over the patch or slot region, the surrounding electromagnetic field distribution is altered, resulting in a change in the effective From Figure 3.

Because the resonant frequency is inversely proportional to the square root of the effective permittivity, any increase in dielectric loading leads to a downward frequency shift:

$$f' = \frac{f_0}{\sqrt{\varepsilon'_{\text{eff}}}}$$

Where, $f'$is the loaded resonant frequency, f is the resonance in air, and ε' is the modified effective permittivity.

Water (εr ≈ 78) produces a significantly larger dielectric loading effect than ice (εr ≈ 3.2), resulting in a more pronounced frequency shift than that of ice. Therefore, by analyzing the shift in the resonant frequency, the antenna can distinguish between water and ice through simulation.

HFSS SIMULATION RESULTS AND ANALYSIS

For Cross-Slot Antenna with Rectangular Patch 3.1.S-Parameter Plot

The S-parameters describe how Radio Frequency (RF) or microwave signals behave in a network, particularly the amount of power reflected and transmitted at different ports from Figure 4.

Antenna in Air Case

The simulated S11 response under air conditions exhibited a strong fundamental resonance near 5.5 GHz with excellent impedance matching (S11 < −30 dB). A secondary resonance was also observed at approximately 4.7 GHz owing to the slot–patch coupling effects. This air response serves as a baseline reference for evaluating the dielectric loading under water and ice conditions from Figure 5.

Under single-layer water loading, the resonant frequency shifted downward from 5.56 GHz (air case) to approximately 5.01 GHz owing to the high dielectric constant of water. The magnitude of S11 slightly improved compared to that under air conditions, indicating dielectric loading effects. This significant frequency shift confirms the strong sensitivity of the proposed antenna to water detection from Figure 6.

Ice as Dielectric Substrate

For the ice layer, the primary resonance was observed near 5.56 GHz with an S11 of approximately −15 dB. Compared to the air case (5.55 GHz), only a slight frequency shift was observed owing to the relatively low permittivity of ice (εr ≈ 3.4). This small shift, in contrast to the significant shift caused by water, demonstrates the capability of the antenna to distinguish between water and ice based on dielectric loading from Figures (7-9).

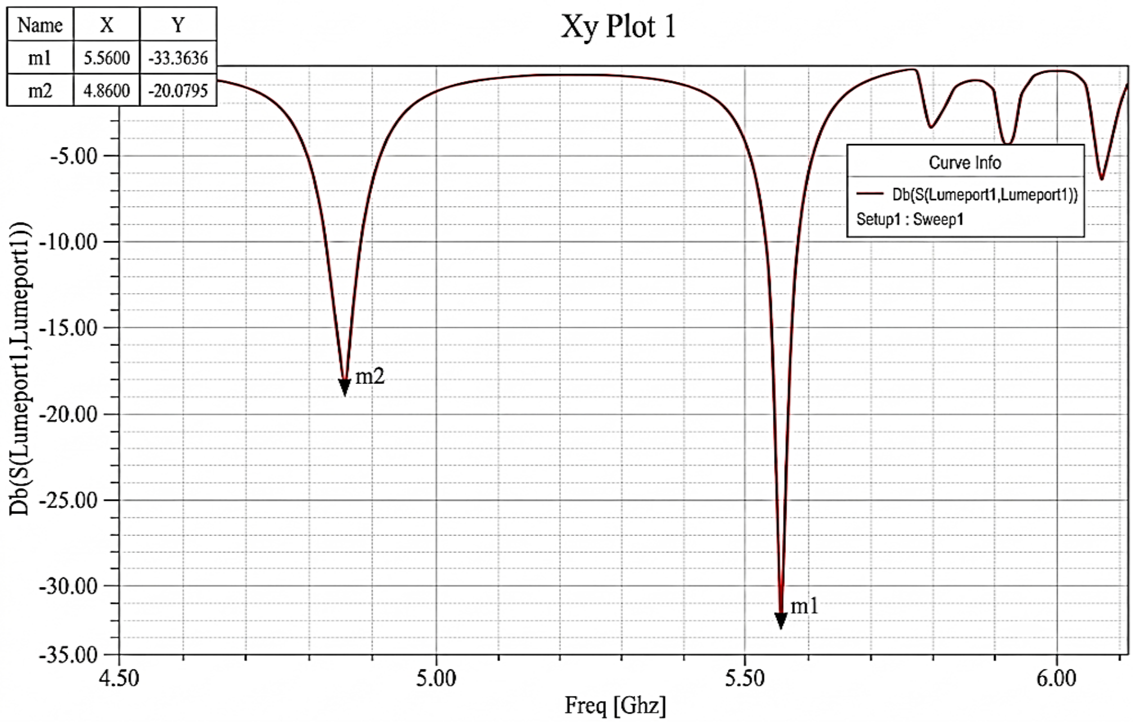

Figure 4. S-Parameter (return loss) cross-slot antenna in air case. 1 mm thickness.

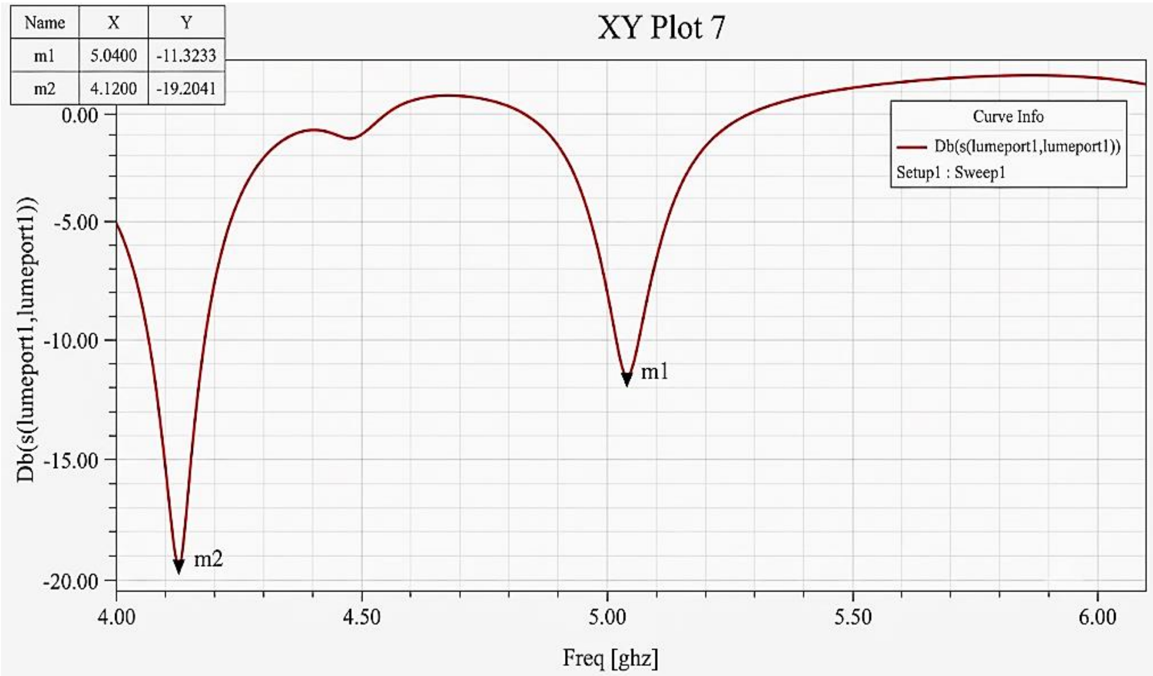

Figure 5. S-parameter (return loss) in air case.

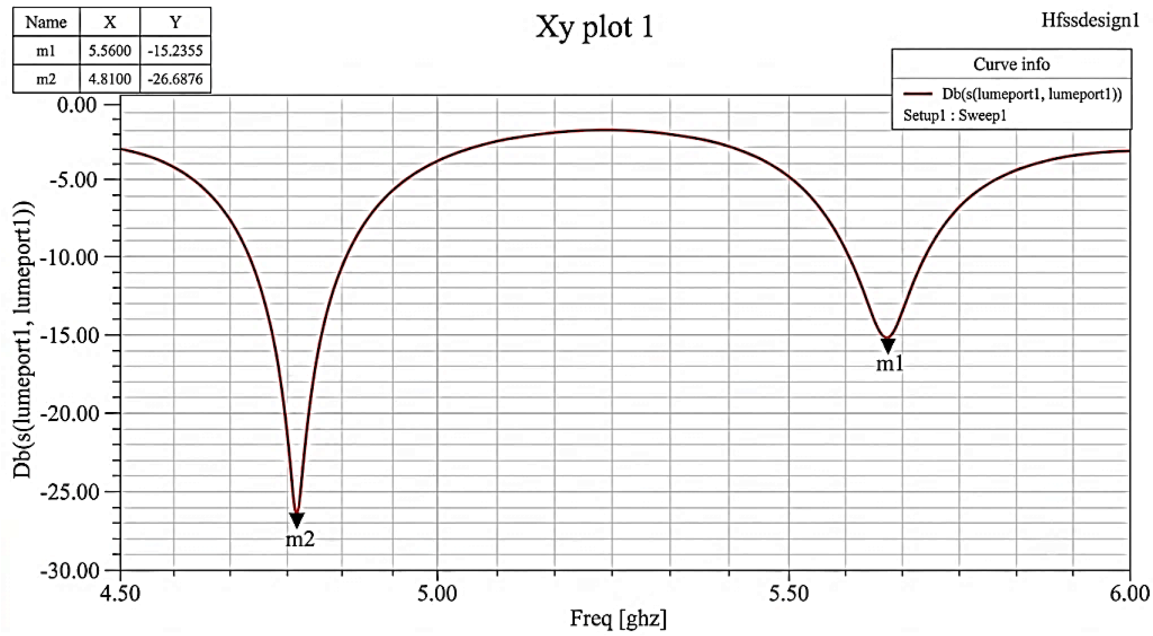

Figure 6. Return loss in case of 1 mm ice layer.

VSWR Plots

The voltage standing wave ratio (VSWR) is a measure of the impedance matching between the antenna and transmission line from Figure 8.

The VSWR plots for the cross-slot antenna for the air, water, and ice cases are shown in Figures 5–7, respectively.

Observing Antenna Performance with Different Thicknesses of Water and Ice Layers

The antenna performance was evaluated by placing ice and water layers over the structure and analyzing the S_{11} characteristics at approximately 5.8 GHz. The results show that the resonant frequency

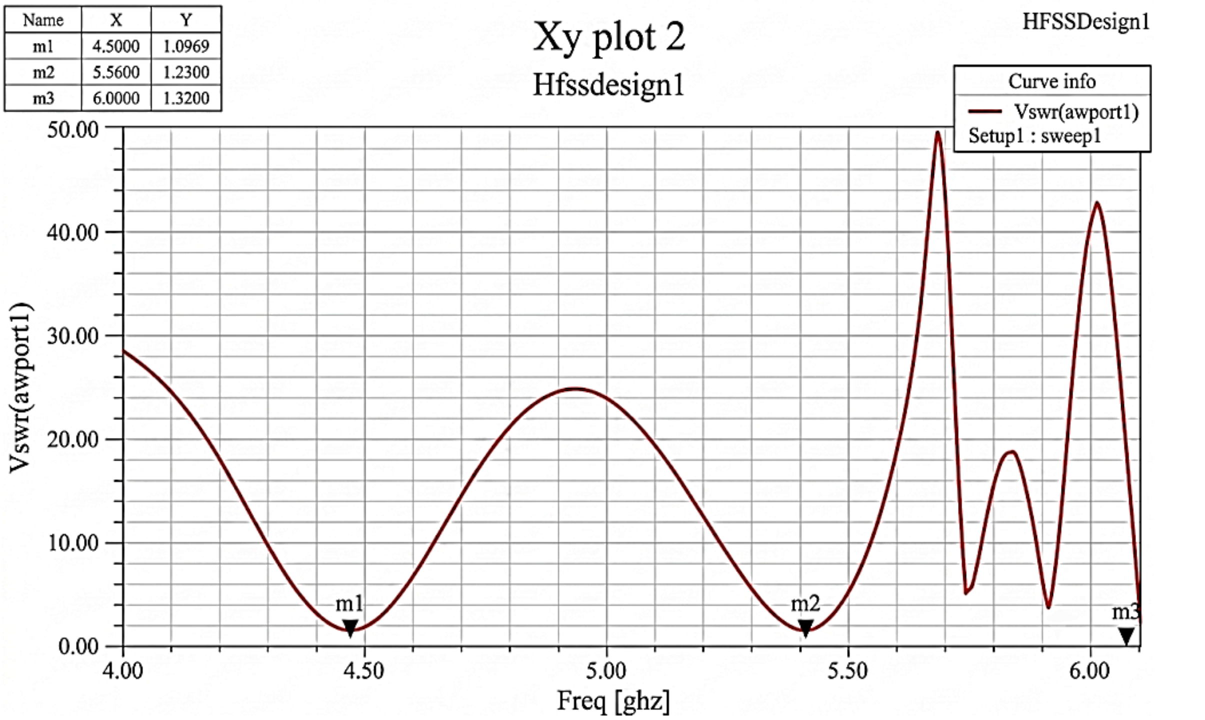

Figure 7. VSWR (1.04) for air case.

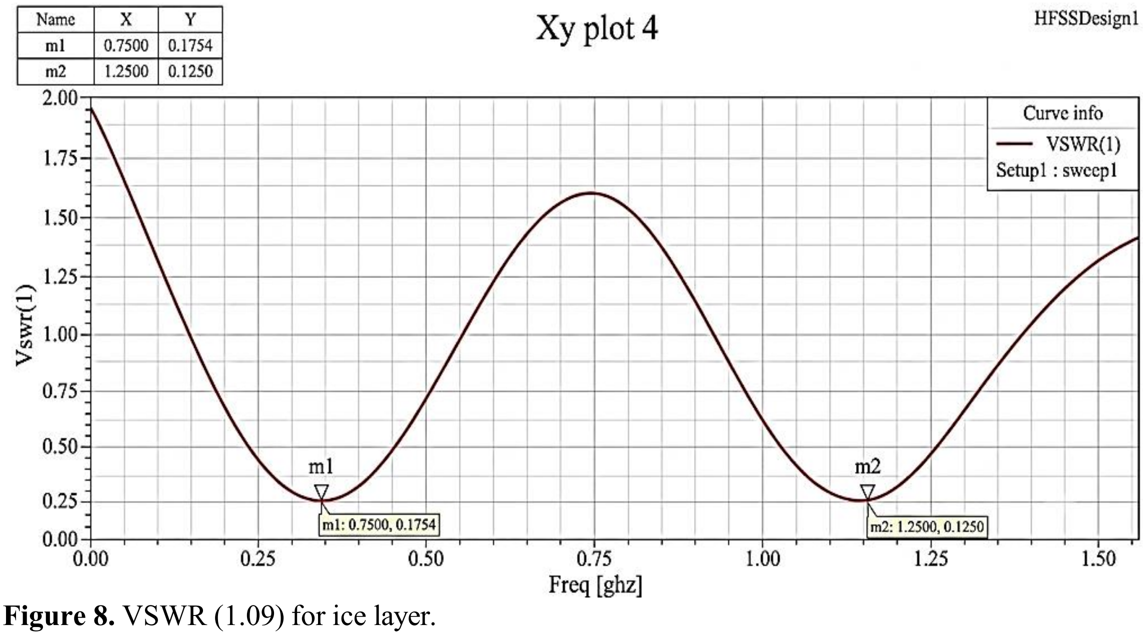

Figure 8. VSWR (1.09) for ice layer.

shifts in both cases as the layer thickness increases; however, the shift is significantly larger for water than for ice. This is because water has a much higher dielectric constant and loss tangent than ice, resulting in stronger from electromagnetic interactions Figure 9.

In terms of return loss, the ice layer exhibits deeper S_{11} minima (up to –30 to –40 dB), indicating better impedance matching, whereas the water layer shows comparatively shallower nulls (approximately –18 to –20 dB). Additionally, water introduces higher dielectric losses, reducing the antenna efficiency more than ice. Overall, the antenna demonstrated a clear differentiation between ice and water, confirming its suitability for ice–water discrimination sensing applications Figure 10.

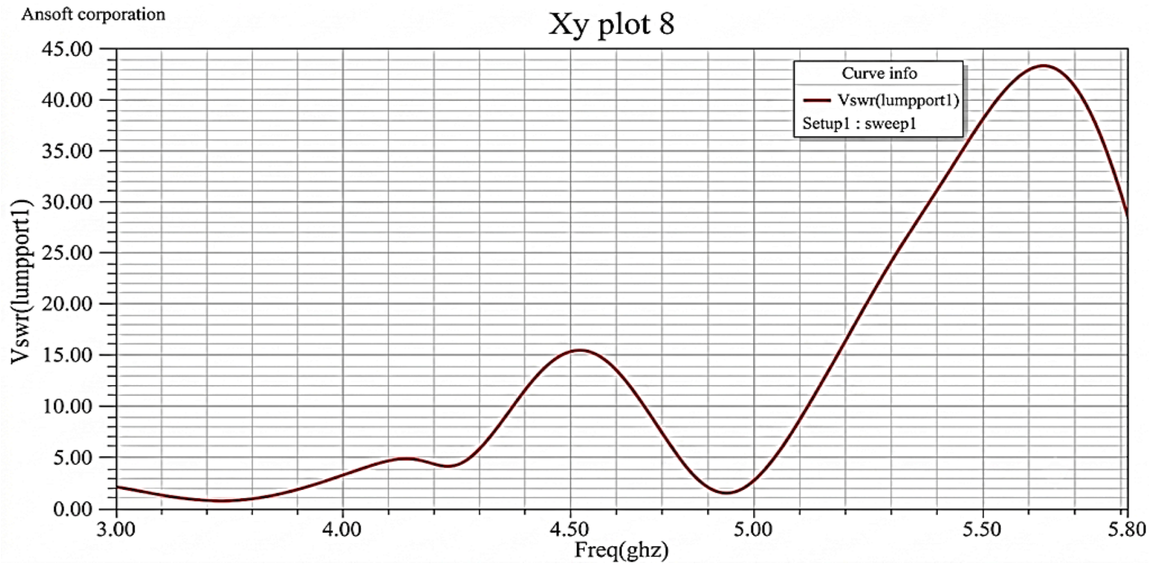

Figure 9. VSWR (1.8) for water layer.

The resonant frequency of the antenna decreased as the thickness of both the ice and water layers increased from 0.5 to 1.5 mm. For the ice layer, the frequency shifted slightly from approximately 5.56 GHz (0.5 mm) to 5.48 GHz (1.5 mm), showing a moderate downward shift with deeper return loss values up to –30 dB. In contrast, the water layer causes a much larger frequency shift, decreasing from approximately 5.04 GHz (0.5 mm) to 4.12 GHz (1.5 mm) owing to its high dielectric constant Figure 11. Additionally, the return loss in the water case is comparatively less deep than that in ice, confirming that water produces stronger frequency perturbation but higher dielectric losses (Table 1).

For the ice-loaded case, the radiation pattern closely resembled that of the unloaded antenna, maintaining symmetry and beam orientation. The minor variation in the lobe magnitude indicates a low dielectric loss, resulting in a relatively preserved gain and radiation efficiency, as shown in Figure 12.

In contrast, the water-loaded case showed a noticeable reduction in radiation intensity and slight beam distortion, as shown in Table 2. This degradation is attributed to the high dielectric constant and conductivity of water, which increase the surface current attenuation and dielectric losses. Consequently, gain reduction and slight beam broadening were observed, as shown in Figure 13.

Despite these variations, the antenna maintained acceptable radiation characteristics in both cases, validating its suitability for simultaneous sensing and wireless communication at 5.8 GHz, as shown in Figure 14.

Radiation Pattern

The simulated far-field radiation patterns of the proposed antenna at 5.8 GHz under water and ice loading conditions are presented in Figures 10 and 11, respectively. In both cases, the antenna exhibited predominantly broadside radiation behavior with the main lobe directed normal to the patch surface, confirming the stable directional performance shown in Figure 13.

Table 1. A parameter comparison for both water and ice.

Parameter	Ice layer	Water layer
Resonant Frequency	Slight shift from original 6 GHz	Larger shift from 6 GHz
Frequency Shift Magnitude	Moderate	Significant
S_{11} (Return Loss) Depth	Deep nulls (≈ –30 dB to –40 dB)	Moderate nulls (≈ –18 dB to –20 dB)
Impedance Matching	excellent matching	Good matching
Stability at 5.8 GHz	More stable	More variation

Table 2. A parameter comparison for both water and ice.

Layer type	Thickness (mm)	Resonant frequency (GHz)	Frequency shift (GHz)	Return loss (dB)
Ice	0.5 mm	≈ 5.56	↓ 0.24	≈–15 dB
	1 mm	≈ 5.52	↓ 0.28	≈ –26 dB
	1.5 mm	≈ 5.48	↓ 0.32	≈ –30 dB
Water	0.5 mm	≈ 5.04	↓ 0.76	≈ –11 dB
	1 mm	≈ 4.69	↓ 1.11	≈ –19 dB
	1.5 mm	≈ 4.12	↓ 1.68	≈ –19 dB

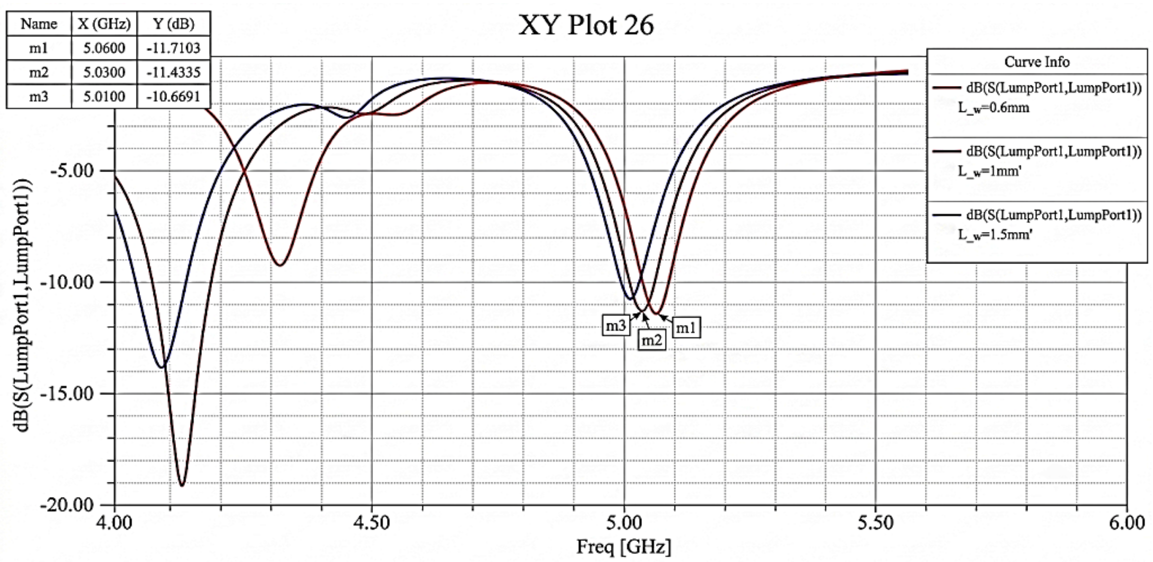

Figure 10. Simulated far-field radiation patterns of the proposed antenna at 5.8 GHz with different ice layer thicknesses (0.5 mm, 1.0 mm, and 1.5 mm).

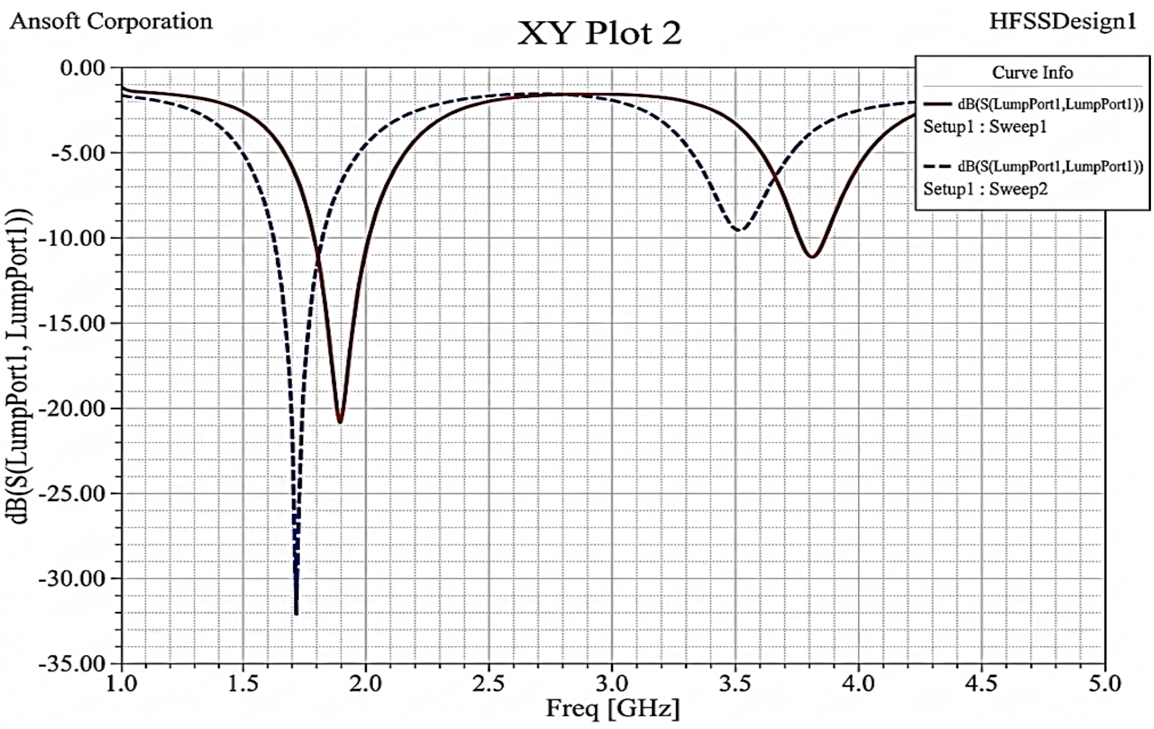

Figure 11. Simulated far-field radiation patterns of the proposed antenna at 5.8 GHz with different water layer thicknesses (0.5 mm, 1.0 mm, and 1.5 mm).

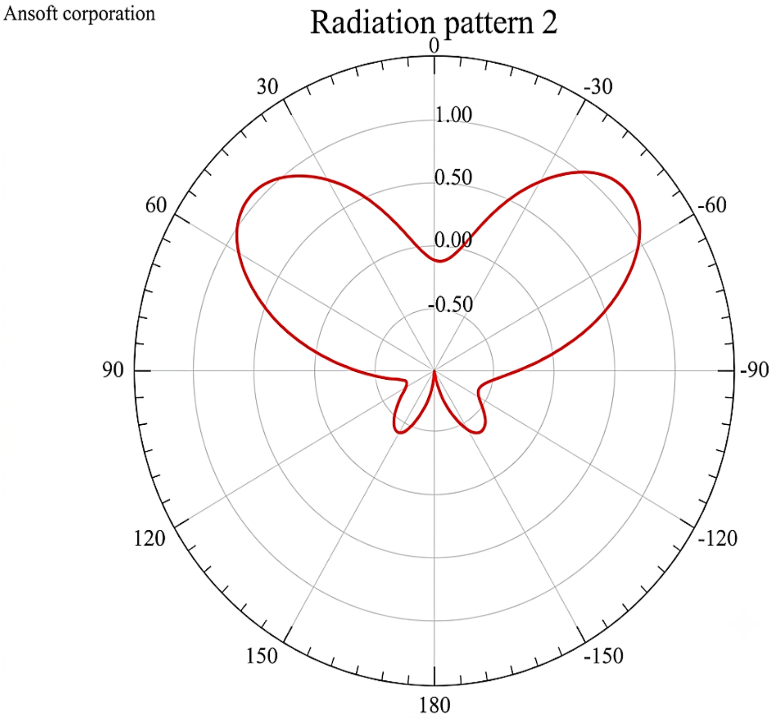

Figure 12. Radiation pattern for adding a water layer.

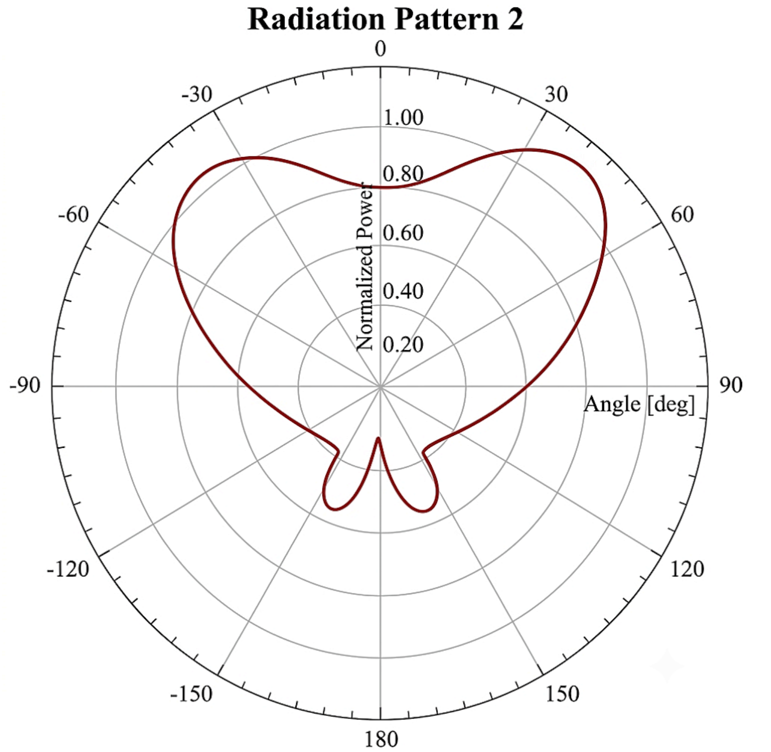

Figure 13. Simulated far-field radiation pattern of the proposed antenna at 5.8 GHz with an ice loading condition, demonstrating stable broadside radiation performance.

D Polar Plots

The simulated radiation patterns at 5.8 GHz demonstrated a significant variation in the gain characteristics between the ice and water media. The ice medium exhibited a higher peak gain (~3.7) with a pronounced main lobe, indicating a lower dielectric loss and reduced attenuation. In contrast, the

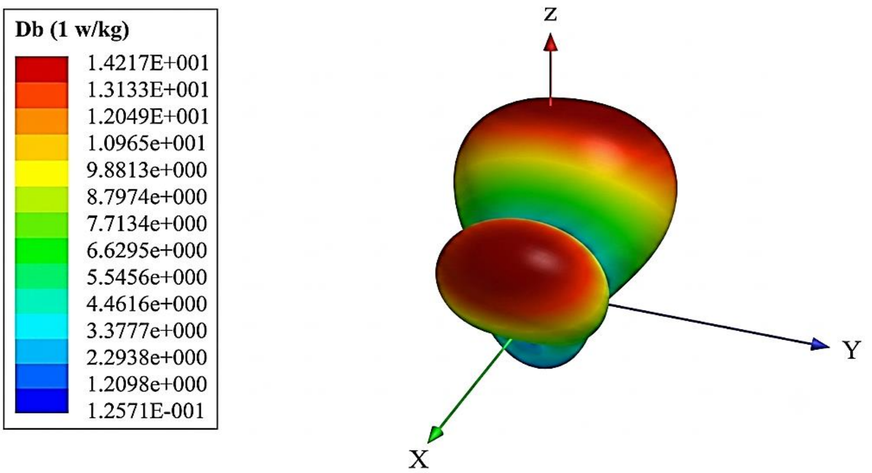

Figure 14. 3D polar plots for water layer.

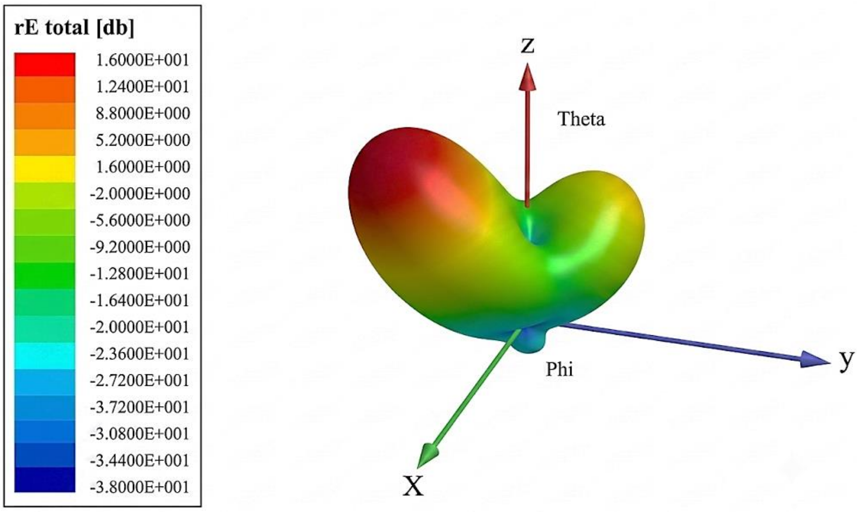

Figure 15. 3D polar plots for ice layer.

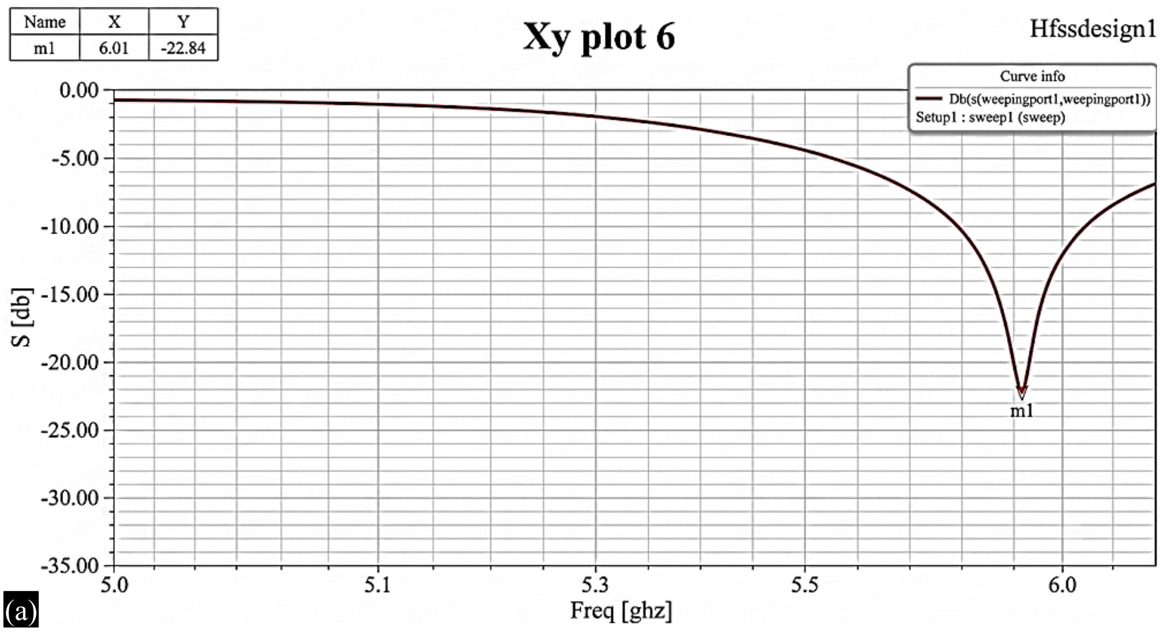

Figure 16. S-parameter.

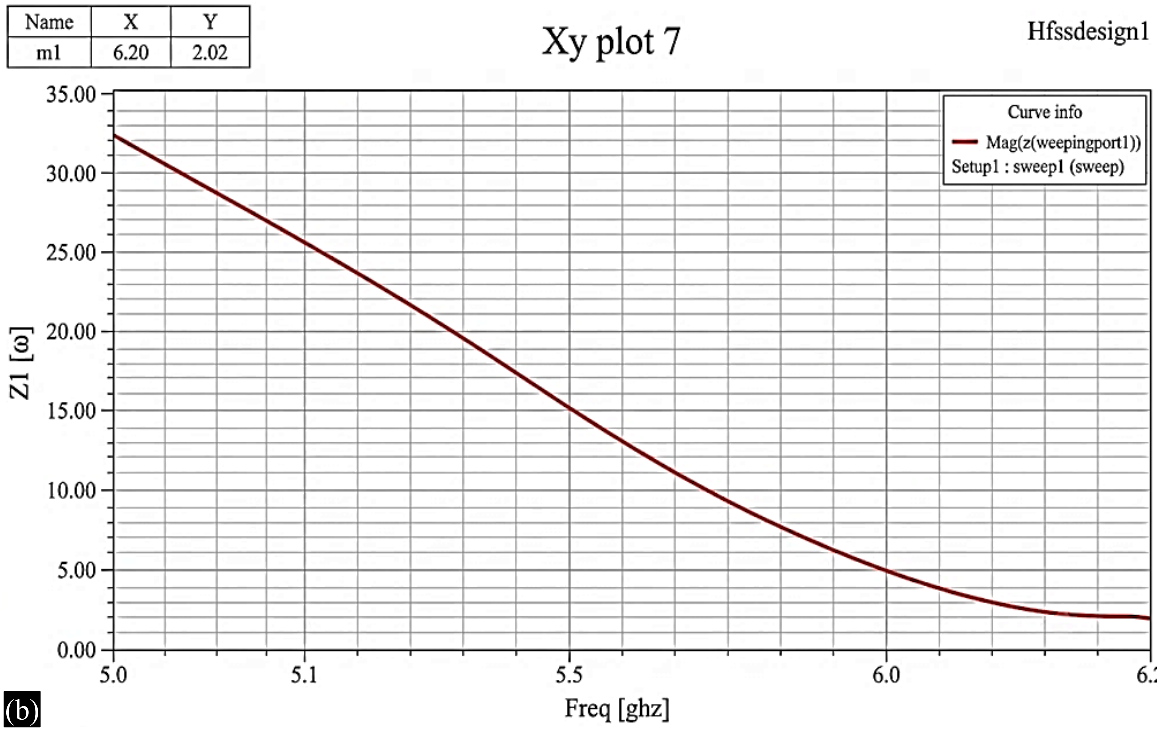

(b)

Figure 16. VSWR plot.

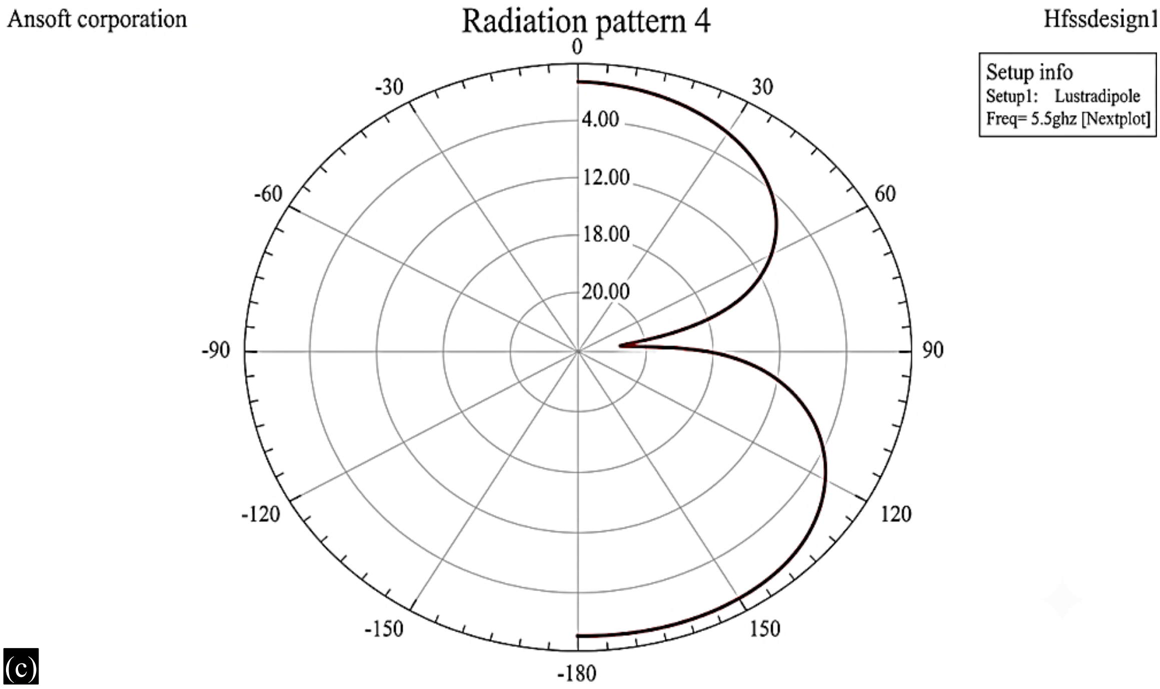

(c)

Figure 16. Gain plot.

water medium showed a substantially reduced maximum gain (~0.66), corresponding to an approximate 72% reduction in peak gain, as shown in Figure 15. This reduction is primarily attributed to the high dielectric constant, increased conductivity, and strong dipole relaxation losses of water at microwave frequencies, resulting in considerable electromagnetic energy absorption and reduced radiation efficiency. The marked gain contrast between the two media confirms the strong electromagnetic sensitivity to the phase transition, thereby validating the effectiveness of the proposed configuration for microwave-based ice–water sensing applications at 5.8 GHz, as shown in Figures 16 (a-d).

For Cross-Slot Antenna with Circular Patch

The proposed cross-slot-coupled circular patch antenna achieved strong impedance matching at 6.34 GHz with a minimum return loss of –31 dB and a VSWR close to unity. The radiation pattern exhibited stable broadside characteristics from Figures a–d. The 3D gain distribution confirmed a peak realized gain of approximately 1.7 dBi. The cross-slot enhances electromagnetic coupling and improves the impedance matching. Overall, the antenna demonstrates stable radiation and suitability for C-band sensing applications.

APPLICATIONS OF CROSS-SLOT MICROSTRIP PATCH ANTENNA

C-Band Wireless Sensor Networks

Operating at approximately 5.8–6.3 GHz, the antenna can be used in environmental monitoring, IoT sensing nodes, and smart infrastructure systems, where stable radiation and good impedance matching are required.

Water Detection Sensors

The antenna can detect changes in the dielectric properties caused by the presence of water, producing a measurable resonant frequency shift.

Ice Accretion Monitoring

It is suitable for detecting ice formation on surfaces such as aircraft wings, wind turbines, and power lines owing to permittivity variation.

Structural Health Monitoring

Enables moisture intrusion detection in buildings, bridges, and composite materials.

Snow/Ice Thickness Measurement

Frequency and return loss variations can be correlated to ice layer thickness.

Smart Road Safety Systems

They can be integrated into pavement sensors to identify icy road conditions in real time (Table 3).

The impedance bandwidth of the rectangular cross-slot–patch antenna was 30 MHz (5.54–5.57 GHz), corresponding to a fractional bandwidth of 0.54%.

The circular patch configuration achieved a wider bandwidth of 100 MHz (5.75–5.85 GHz), corresponding to a fractional bandwidth of 1.72% (Table 4).

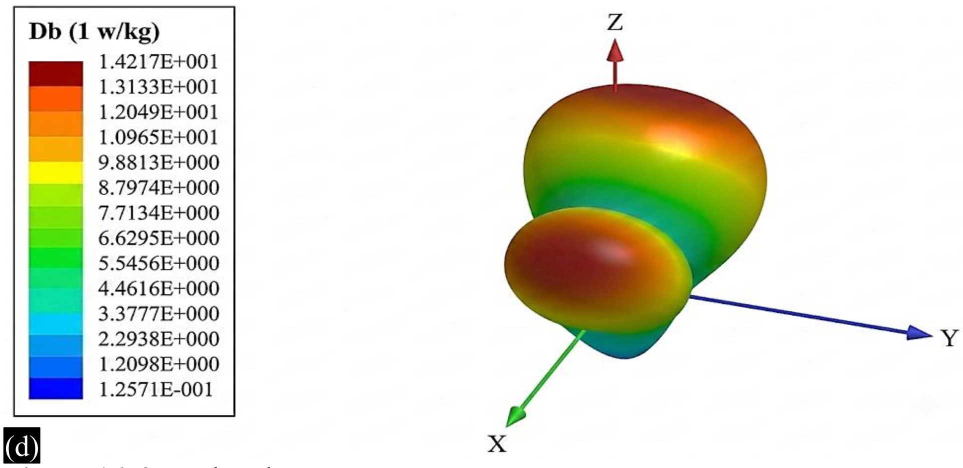

(d)

Figure 16. 3D polar plot.

Table 3. Conventional patch antenna.

S.N.	Parameter	Conventional patch antenna	Cross-slot coupled patch antenna
1.	Resonant frequency	5.8 GHz	5.8 GHz (shift due to slot coupling)
2.	Polarization	Linear	Circular polarization (via cross-slot coupling)
3.	Sensitivity to dielectric loading	Moderate	High (enhanced field interaction)
4.	Gain	Moderate	Improved radiation performance
5.	Detection capability	Limited sensing accuracy	Effective detection of water, ice, and frost
6.	Structural complexity	Single-layer, simple feed	Dual-layer substrate with cross-slot feed

Table 4. Cross-slot antenna with circular patch.

S.N.	Parameters	Cross-slot antenna with circular patch	Cross-slot antenna with rectangular patch
1.	Frequency	6 GHz	5.8 GHz
2.	Antenna dimensions	L1 = 9 mm, L2 = 6.5 mm. W = 1 mm	L1, L2 = 10 mm, W = 2.5 mm
3.	Ground plane size	40 mm × 40 mm	40 mm × 40 mm
4.	Bandwidth	100 MHz	30 MHz
5.	Gain	1.7 dBi	3.7 dBi for ice, -1.8 dBi for water
6.	Directivity	2.67 dB	4.7 dB for ice layer
7.	Efficiency	73%	80% for ice layer

CONCLUSION

Both cross-shaped slotted microstrip patch antennas were successfully designed for wireless sensing applications. The antenna demonstrated high sensitivity to dielectric variations through resonant frequency shifts. The cross-slot improves the near-field electric intensity and enhances the sensing performance without significantly affecting the radiation characteristics. The proposed antenna offers a compact, low-cost, and efficient solution for environmental monitoring.

REFERENCES

1. Chen J, Berg M, Rasilainen K, Siddiqui Z, Leinonen ME, Pärssinen A. Broadband cross-slotted patch antenna for 5G millimeter-wave applications based on characteristic mode analysis. IEEE Trans Antennas Propag. 2022;70(12):11277-11292. doi:10.1109/TAP.2022.3209217.
2. Sagar R, Singh Rajawat SP, Jain R, Thakare VV. Microstrip fed hexagonal shaped cross-slotted antenna for N257 band applications. Proceedings of the IEEE International Conference on Interdisciplinary Approaches in Technology and Management for Social Innovation (IATMSI). Vol. 3; 2025. p. 1-4. doi:10.1109/IATMSI64286.2025.10985073.
3. Kumar AS, Avinag U, Teja AP, Babu GN, Charan AS. High gain tri-band patch antenna using crossed-slot and complementary split ring resonator structure. AIP Conference Proceedings. 2024;020063. doi:10.1063/5.0212502.
4. Mekki K, Necibi O, Boussetta C, Gharsallah A. Miniaturization of circularly polarized patch antenna for RFID reader applications. Eng Technol Appl Sci Res. 2020;10(3):5655-5659. doi:10.48084/etasr.3445.
5. Krishan R. A novel cross-slotted dual-band fractal microstrip antenna design for Internet of Things (IoT) applications. In: Advanced Sensing in Image Processing and IoT. Boca Raton (FL): CRC Press; 2022. p. 245-254. doi:10.1201/9781003221333-13.
6. Samsuzzaman M, Islam MT, Faruque MRI. Dual-band multi slot patch antenna for wireless applications. J Telecommun Inf Technol. 2013;(2):19-23. doi:10.26636/jtit.2013.2.1211.
7. Verma MK, Kanaujia BK, Saini JP, Saini PS. A broadband circularly polarized cross-slotted patch antenna with horizontal meandered strip (HMS). Frequenz. 2020;74(5-6):191-199. doi:10.1515/freq-2019-0113.
8. Rashid D, Kumar S, Kanaujia BK, Gautam AK. Compact cross shaped slit circularly polarized microstrip antenna for GNSS applications. Proceedings of the International Conference on Computational Intelligence and Communication Networks (CICN); 2014. p. 30-32. doi:10.1109/CICN.2014.18.

9. Anim K, Shin GH, Jung YB. Dual-resonant stacked linear array of cross-slotted patches for small SAR satellites. IEEE Trans Antennas Propag. 2021;69(6):3584-3587. doi:10.1109/TAP.2020.3030534.
10. Feng G, Chen L, Xue X, Li N, Shi X. Broadband CP crossed-stepped-dipole antenna incorporating a cross slotted square patch. IET Microw Antennas Propag. 2019;13(3):340-345. doi:10.1049/iet-map.2018.5254.
11. Wang M, Zhang H, Hu N, Xie W, Chen S, Chen Z. A wideband circularly polarized filtering array antenna using dual-layer circular cross slotted patch. 2024 18th European Conference on Antennas and Propagation (EuCAP), Glasgow, United Kingdom. 2024. p. 1-3. doi:10.23919/EuCAP60739.2024.10501563.
12. Gundala S, Srinivasa Baba VS, Srigada S, Pooja N, Preethililly K, Talusani SK. Cross slotted antenna at X band for wireless applications. Proceedings of the IEEE Wireless Antenna and Microwave Symposium (WAMS); 2024. p. 1-7. doi:10.1109/WAMS59642.2024.10527953.
13. Margaret DH, Anith S, Duraisamy M, Muneeswaran KPK. Cross slot antenna with open ended truncated patch feed for ultra wide band applications. 2009 International Conference on Control, Automation, Communication and Energy Conservation, Perundurai, India. 2009. p. 1-6.

